## PAPER

Check for updates

# Diesel exhaust particles modulate bone remodeling and worsen osteoporosis: *in vitro* and *in vivo* investigations†

Vaishnavi N,[a] Saravanan Sekaran,[b] Renugaa Suresh babu,[a] Swathi Sudhakar [ID] *[a] and Selvaraj Vimalraj [ID] *[a]

Air pollution poses significant risks to public health, with diesel exhaust particles (DEP) contributing to a variety of systemic effects, including potential impacts on bone metabolism. This study investigates DEP's osteogenic and bone toxic effects using both *in vitro* pre-osteoblast models and *in vivo* Zebrafish models under healthy and osteoporotic conditions. Pre-osteoblasts treated with DEP exhibited enhanced calcium deposition and upregulated osteogenic markers, including Runx2 and type I collagen, at 25–50 µg ml$^{-1}$ concentrations. Zebrafish larvae and adult models demonstrated similar concentration-dependent responses, with increased mineralization observed at lower DEP doses and reduced mineralization at higher concentrations (≥100 µg ml$^{-1}$). Notably, DEP exposure in osteoporotic Zebrafish consistently impaired bone regeneration and fracture healing, as evidenced by diminished calcium deposition, reduced alkaline phosphatase activity, and increased osteoclast activity. Mechanistically, DEP was shown to act through the aryl hydrocarbon receptor (AhR) pathway, disrupting the balance between osteoblast and osteoclast activity. At higher doses or under pathological conditions such as osteoporosis, DEP significantly impairs bone regeneration, delays fracture healing, and promotes bone resorption. The distinct responses elicited by these particles in healthy compared to osteoporotic bone highlight their dualistic nature and underscore the need for condition-specific investigation. This research underscores the importance of the risks associated with chronic DEP exposure in vulnerable populations. Future studies should focus on elucidating the molecular mechanisms underlying DEP's biphasic effects and exploring mitigation strategies for its adverse impacts on bone health.

## 1. Introduction

Air pollution is one of the most prevalent types of environmental pollution, with numerous adverse effects on the environment and living organisms. There are various sources; among which, vehicular emissions are the primary contributors, releasing numerous particles, including ultrafine particles, into the atmosphere. People who work near highways or around diesel-powered equipment are at higher risk of exposure to diesel exhaust. As diesel engines are widely preferred over gasoline engines for various reasons, they unfortunately emit harmful pollutants that pose substantial health risks.[1] The real-time combustion processes result in a mixture of particulate matter and other pollutants. Diesel exhaust contains solid, liquid, and gas-phase pollutants such as carbon gases, particulates, hydrocarbons (*e.g.*, benzene, formaldehyde), and heavy metals like lead and cadmium. Its exact composition varies based on factors such as engine type, operating conditions, lubricating oil, additives, emission control systems, and fuel composition. Diesel emissions predominantly consist of a nonpolar fraction (57%), a moderately polar fraction (9%), and a polar fraction (32%), with the remainder being unrecoverable.[2] Over 90% of diesel exhaust particulates are ultrafine particles (<1 µm) classified as PM$_{2.5}$ and PM$_{10}$ by the Environmental Protection Agency (EPA) and World Health Organization (WHO); their deep tissue penetration and interaction with cellular pathways have raised interest in DEP's biphasic effects on bone metabolism under both healthy and osteoporotic conditions. In the present study, we utilized diesel exhaust particles (DEPs) directly collected from the exhaust outlets of heavy-duty diesel engine buses operating under real-world conditions. This approach ensures environmental relevance and more accurately reflects human exposure scenarios compared to using synthetic or laboratory-generated particles. By employing these real-world DEP samples, we aimed to investigate their biphasic effects on bone metabolism using

*[a]Department of Applied Mechanics and Biomedical Engineering, Indian Institute of Technology-Madras, Chennai-600 036, Tamil Nadu, India. E-mail: swathi.s@iitm.ac.in; vimalraj@iitm.ac.in*

*[b]Department of Prosthodontics, Saveetha Dental College and Hospitals, Saveetha Institute for Medical and Technical Sciences, Chennai-600077, Tamil Nadu, India*

† Electronic supplementary information (ESI) available. See DOI: https://doi.org/10.1039/d5na00254k

both zebrafish and *in vitro* osteoblast models. This study bridges the gap between environmental exposure and biological outcomes, offering novel insights into how ambient particulate matter may influence bone formation and remodeling under physiological and pathological conditions.

The health risks associated with diesel exhaust particles (DEP) are significant. These particles can infiltrate the body, enter the bloodstream, and cross the blood–brain barrier, affecting multiple organs and systems. Prolonged exposure to DEP leads to both acute and chronic health effects, including eye and nose irritation, altered lung function, airway inflammation, headache, lethargy, and nausea. Research has shown that even healthy individuals can experience deep inflammatory changes in the airways before any alterations in pulmonary function are detected. Numerous epidemiological studies worldwide have linked ambient air particulate levels to adverse health outcomes, such as death, asthma exacerbations, chronic bronchitis, respiratory infections, ischemic heart disease, and stroke.[3,4] The carcinogenic and mutagenic potential of DEP has been extensively studied, with evidence from both human and animal studies. Additionally, DEP exposure has been associated with neurological effects, including neurodegenerative diseases like Alzheimer's and Parkinson's, as well as impaired cognitive performance.[5] Despite extensive research on other systems, the effects of air pollution, particularly DEP exposure, on bone metabolism remain underexplored. This study aims to investigate the physiological and remodeling effects of DEP on bone using Zebrafish (Danio rerio) as an animal model using scale regeneration and tail injury studies.[6] To analyze the activity of Osteoblast and osteoclast activity, biomarker analyses were performed by exposing adult zebrafish to controlled amounts of DEP. In this study, zebrafish were chosen as an animal model to test the effects of diesel exhaust particles and the PM present in them. It has many advantages compared to other animal models because of its genetic similarity, easy handling, and rapid breeding capabilities.[7] Other advantages of choosing as a bone model are due to their vertebrate nature and the similarity of their skeletal physiology to mammals. Zebrafish exhibit both dermal/intramembranous and chondral/endochondral ossification, essential processes in bone formation and remodeling.[8] The translucency of Zebrafish larvae allows for *in vivo* imaging of cellular behavior during skeletal development. Additionally, various approaches have been developed to study bone mineralization, formation, regeneration, and osteoblast-osteoclast interactions in Zebrafish. In this study, we investigated the toxic effects of diesel exhaust particles (DEP) on zebrafish and *in vitro* osteoblast cells to better understand their impact on bone development. While previous research has explored DEP toxicity, studies demonstrating the biphasic nature of particulate matter on bone biology remain limited. To address this gap, we conducted both qualitative and quantitative assays, assessing gene expression, calcium mineralization, and deposition following DEP exposure. DEP samples were collected from diesel vehicle exhaust pipes, providing a relevant real-world source of particulate matter. Our findings reveal changes in mRNA expression and bone matrix deposition, offering novel insights into how air pollution may simultaneously impair and stimulate aspects of bone formation and remodeling. This dual effect has not been clearly demonstrated before and highlights the complexity of environmental pollutants on skeletal health.

## 2. Materials and methods

### 2.1 DEP collection, preparation and characterization

Diesel Exhaust Particles (DEP) were collected directly from the exhaust pipes of diesel engine vehicles (specifications to be provided Diesel exhaust particles (DEPs) were collected from the exhaust pipe outlets of heavy-duty diesel engine buses (Ashok Leyland) operated under real-world conditions within the Indian Institute of Technology Madras (IITM) campus. These buses are part of a fleet routinely maintained at the IITM bus depot and fueled with standard commercial high-speed diesel (HSD). The engines were typically run at low to moderate load conditions for durations ranging from 30 minutes to 2 hours. During operation, persistent emissions of black exhaust gases, consisting of combustion-derived particulates including nanoscale soot agglomerates, were observed. Over time, these particulates are deposited along the interior walls of the exhaust pipe outlets due to thermophoretic and diffusional transport mechanisms. Soot samples were carefully scraped using sterile stainless-steel spatulas from a 5–10 cm region near the exhaust tip, where visible deposition was prominent. The collected material was immediately transferred into sterile 50 mL polypropylene Falcon™ tubes and stored at room temperature in airtight conditions until further use. These DEPs were used as the primary material for all subsequent physicochemical and morphological characterization procedures). For preparation, DEP samples were dissolved in 0.1% dimethyl sulfoxide (DMSO) and subjected to vortex mixing for 30 minutes to ensure uniform dispersion. To evaluate the physical and chemical properties of DEP, a comprehensive characterization was performed. The morphology and elemental composition of DEP were analyzed using scanning electron microscopy (SEM) integrated with energy-dispersive X-ray (EDX) spectroscopy.[9] SEM imaging was conducted at a magnification of $1\,000\,00\times$ using a 5 kV voltage setting, providing detailed surface morphology insights. Elemental analysis through EDX was carried out at 2 spots on the DEP surface to determine the relative concentration of elements present. This characterization provided a detailed understanding of DEP properties, facilitating the evaluation of their effects on biological systems.

### 2.2 Cell culture

MC3T3 pre-osteoblast cells, procured from the National Centre for Cell Science (NCCS), Pune, India, were cultured in standard tissue culture plates and maintained in Alpha Minimum Essential Medium (Alpha MEM) supplemented with 10% fetal bovine serum (FBS), antibiotics, and antimycotics (Invitrogen, USA). The cells were incubated in a humidified atmosphere containing 5% $CO_2$ at 37 °C until they reached confluency, with experiments conducted at 24, 48, and 72 hours post-culturing.

DEP were prepared at a stock concentration of 1 mg ml$^{-1}$ by dispersing them in 0.1% dimethyl sulfoxide (DMSO) (Sigma Aldrich, USA). Cells were treated with varying concentrations of DEP to assess dose-dependent effects. Morphological changes in the cells were observed and documented using a light microscope to evaluate potential alterations induced by DEP exposure.

## 2.3 MTT assay

Cytotoxicity tests were performed by colourimetric MTT assay[10] to assess the impact of diesel exhaust particles. The cell was seeded in equal concentrations/density in 6 well plates and was allowed to adhere. Following adherence, the cells were treated with increasing concentrations of DEP such as 10, 25, 50, 100, and 200 μg ml$^{-1}$ for 20 hours. 0.1% DMSO was used as a control. These concentrations were chosen in order to look at how different DEP dosages might impact the viability of cells. After a 20-hours treatment period, a 3-(4,5-dimethylthiazol-2-yl)-2,5-diphenyltetrazolium bromide (MTT) assay was performed. The medium was removed and the cells were washed with PBS. Then cells were incubated with 20 μL of 5 mg mL$^{-1}$ MTT solution for 4 h at 37 °C to enable the formation of formazan crystals. Subsequently, the medium was cautiously aspirated to remove excess MTT solution, and 100 μL of DMSO was added to each well to solubilize the formazan crystals formed by metabolically active cells. The absorbance of the resultant solution was measured at 570 nm using a microplate reader. The absorbance readings were normalized to those obtained from untreated control wells to calculate cell viability percentages.

## 2.4 Alizarin red staining

To assess the impact of DEP on osteogenic differentiation and calcium deposition, Alizarin Red S staining was performed.[11,12] First, the culture medium was carefully removed and cells were washed with phosphate-buffered saline (PBS). Then the cells were fixed with 4% paraformaldehyde for 30–45 min to ensure cellular fixation. Subsequently, the fixed cells were washed twice with distilled water to remove residual fixative. Next, the cells were treated with 1 mL of 2% Alizarin Red S solution (pH 4.0–4.5) for 10–15 min in the dark. This staining protocol allowed for the visualization of calcium deposits in the cells. Following staining, the cells were thoroughly rinsed to eliminate excess dye and photographed using a suitable imaging system.

## 2.5 Zebrafish maintenance and exposure

The Zebrafish (*Danio rerio*) used in the study was commercially brought and maintained and propagated in our recirculating facility system that continuously filters and aerates the system water to maintain the water quality required for a healthy aquatic environment. The circulating system also helps to filter excess food and fish excreta. Zebrafish were maintained at 27.0 °C ± 1.0 °C under light conditions of 14 h light and 10 h dark supplied with fresh water and an aerator. The Zebrafish were fed a dry diet, and breeding was conducted as required under controlled conditions. The Zebrafish embryos were raised by placing male and female Zebrafish in a smaller tank separated

by a glass divider in between and a mesh bottom overnight to initiate breeding. The glass divider was removed the following morning to allow the natural breeding of fish. Fertilized embryos that settled to the tank's bottom were carefully collected using a pipette and transferred to separate containers for further maintenance. To study the effect of our DEP on diseased fishes. Osteoporosis condition was induced in adult fishes by treating them with dexamethasone at a concentration of 0.5 mg per lit for 10 days.[13] Dexamethasone is known to induce early-stage osteoporotic characteristics in Zebrafish. The osteoporosis-induced fishes were further treated with different concentrations of DEP and the control was 0.1% DMSO. This gives insights into how the diesel exhaust particles affect new bone formation, especially scale regeneration and fin fracture healing in pathologic conditions.

The healthy Zebrafish embryo, larva, and adult fishes were selected and distributed accordingly and exposed to DEP at 0, 25, 50, 100 and 200 μg ml$^{-1}$ for 7 days at 28 °C. The 0.1% DMSO-treated Zebrafish were used as vehicle control. For embryos and larvae, the dead were discarded every day. The mortality and hatching of embryos were recorded daily within every concentration group. The institutional animal ethical committee at Saveetha University, India (BRULAC/SDCH/SIMATS/IAEC/03/2024/03) approved all protocols.

## 2.6 Zebrafish embryo/larva toxicity

The toxicity of DEP on Zebrafish embryos/larvae was tested based on their hatching in each group and were also selected to test their changes in bone formation.[14] 30 embryos were kept in each group. Control groups were maintained in water containing the equivalent quantity of DMSO used for the highest concentration of DEP. The hatching rate was calculated up to 4 dpf (days post-fertilisation). Following the hatching rate, the viability of the larva was also assessed by continuing the larvae treatment for up to 7 dph (days post-hatch), and viability was assessed. To study bone development, the 7dpf larva from each group were collected and fixed on a glass slide using ethanol for Alizarin Red S staining. Each larvae were separately stained with 0.05% of alizarin red for 5 minutes (pH 4.2). The larvae in slides were washed with 0.5% KOH to remove excess stain. The stained larvae were imaged under a fluorescent microscope at excitation wavelength 495 nm to visualize the vertebral bone formation. Images obtained were quantified for bone count.

## 2.7 Scale regeneration in adult zebrafish

To investigate the mineralization patterns of the regenerated scales after treatment with DEP.[15,16] The Zebrafish were anesthetized with ice-cold water (0 °C) to remove the ontogenic scales present on either side of the body by placing them under a light stereomicroscope using forceps. Then the Zebrafish were grouped under various concentrations of DEP. After 7 days of exposure, the fish were taken out to obtain the regenerative scales. The regenerated scales were washed with distilled water and fixed 4% paraformaldehyde, and 3% H$_2$O$_2$ for staining. Then Bone matrix and mineralization profiling studies were evaluated through vital staining in Alcian blue, Alizarin red S,

Calcein, and Von Kossa. Osteoporosis-induced adult fishes were also treated in the same way as mentioned above to study the mineral deposition in the regenerated scales.

## 2.8 Fin fracture model in zebrafish

For studying bone healing, the Zebrafish were anesthetized with ice-cold (0 °C) water. Then, the fish was placed under the stereomicroscope. The injury was created in the tail fin by gently pressing the fine nodes using sterile forceps. Zebrafish tails were fractured and amputated as described previously.[17] The fishes with bone defects were exposed to different concentrations of DEP (0 to 100 $\mu g\ ml^{-1}$) and were maintained for tail fin bone re-union. The control group was treated with 0.1% of DMSO. The calcium mineralization in the fin regions after regeneration was studied by incubating them with 0.05% alizarin red in the dark environment for 15 min followed by rinsing the fishes in the distilled water to remove excess stains. Then the photomicrographs were documented using a fluorescent microscope (Leica Microsystems, Germany). The formation and mineralization of the callus, a critical part of the bone healing process, were visualized and quantified using Image J software. The formation was noticed around the fracture site during day 7. The cellular imaging at the injured site defines the temporal phases of bone repair in fish, focusing on inflammation, chondrogenesis, ossification, and remodeling.

## 2.9 Whole mount staining

Zebrafish were subjected to anesthesia and fixed by incubating them at 42 °C in a shaking plate containing a solution composed of 5% formalin, 5% Triton X-100, and 1% potassium hydroxide for 12–48 hours. This ensured proper fixation of the samples for subsequent analysis. Following fixation, the specimens were immersed in an enhancement solution comprising 20% ethylene glycol, 5% Triton X-100, and 1% potassium hydroxide and kept at 27 °C until they were completely decolorized and became transparent. This solution facilitated the clearing of tissues, enhancing visibility during staining. After this step, the specimens were stained with 0.05% alizarin red S, 20% ethylene glycol, and 1% potassium hydroxide for 30 min. Alizarin red S is a dye commonly used to detect calcium deposits, aiding in the visualization of mineralized tissues. Post-staining, the samples underwent a de-staining process in a clearing solution containing 20% Tween 20 and 1% potassium hydroxide. This step helped in the removal of excess stains and improved clarity for imaging. Subsequently, the samples were stored in glycerol and imaged using a fluorescent microscope. This method of staining was first performed by.[18] The imaging focused on the axial skeletal region to trace and evaluate mineralization. This methodology enabled the visualization and assessment of mineralized tissues in the vertebral region of healthy, normal, and dexamethasone-induced zebrafish. The staining and imaging techniques applied in this assay provided insights into the extent and pattern of mineralization in the axial skeletal area, contributing valuable information regarding bone formation and development in the experimental zebrafish model.

## 2.10 Energy dispersive analysis (EDX) for Ca : P ratio

To investigate the calcium and phosphorus ions in the regenerated scales we performed EDXs microanalysis as described by.[6,19] The collected regenerated scales were washed with phosphate-buffered saline (PBS) to remove dust and other debris. Then the scales were fixed on a glass slide for calcium and phosphorous weight measurement. The fixed scales were then sputter-coated for 120 seconds. Then EDX was taken at 3 different positions on the scales. This will give insights into the Quantification of the EDX signal to estimate the calcium : phosphorus molar ratio roughly.

## 2.11 ALP and TRAP enzyme activity

To investigate the activity of enzymes, the regenerated zebrafish scales were prepared for analysis by careful washing with PBS and ensuring they were free from any contaminants or debris. Then incubated in 100 µl basal lysis buffer solution containing 10 mM Tris pH 7.5, 150 mM NaCl, 1 mM EDTA, and 1% Triton X 100 (Nonionic detergent) for 40 min on ice. Then the solution was centrifuged at 17 400 ×g for 15 minutes at 4 °C. The lysate with pellet was sonicated for a total time of 12 minutes. This was used for performing ALP & TRAP activity measurements according to Chaichit et al.,.[20]

For ALP activity measurement, 10 µl lysate was added to 100 µl of reaction buffer containing 100 mM Tris HCl buffer, pH 9.5 containing 20 mM $MgCl_2$, and 0.1 mM $ZnCl_2$. This incubation step was essential to prepare the scales for subsequent ALP activity assessment. Subsequent Incubation with 20 mM p-nitrophenylphosphate Solution for 1 hour at 28 °C. This solution likely served as a substrate to determine the ALP enzyme activity within the Zebrafish scales. The enzymatic reaction initiated by the addition of p-nitrophenyl phosphate was halted by adding 50 µl of 3 M NaOH. The absorbance of the reaction mixture was then measured at a wavelength of 405 nm using a spectrophotometer or a microplate reader.

For TRAP activity measurement, 10 µl lysate was added to 100 µl of reaction buffer containing 100 mM sodium acetate buffer, pH 5.3 supplemented with 20 mM tartrate. This incubation step was essential to prepare the scales for subsequent TRAP activity assessment. Subsequent Incubation with 20 Mm p-nitrophenylphosphate solution for 1 hour at 28 °C. This solution likely served as a substrate to determine the TRAP enzyme activity within the zebrafish scales. The enzymatic reaction initiated by the addition of p-nitrophenyl phosphate was halted by adding 50 µl of 3 M NaOH. The absorbance of the reaction mixture was then measured at a wavelength of 405 nm using a spectrophotometer or a microplate reader.

## 2.12 Gene expression analysis *via* RT-PCR

Total RNA was isolated using the TRIZOL reagent and quantified using the Nanodrop One spectrophotometer (Thermo Scientific).[21] The Invitrogen reverse transcription kit converted one microgram of the extracted RNA into complementary DNA (cDNA). This cDNA served as the template for quantitative real-

**Table 1** Primer sequences used for real time RT-PCR analysis

| Gene | 5′ → 3′ | Sequence |
|---|---|---|
| m-Runx2 | Forward | CGCCTCACAAACAACCACAG |
| | Reverse | TCACTGTGCTGAAGAGGCTG |
| m-Type1 col | Forward | TAACCCCCTCCCCAGCCACAAA |
| | Reverse | TTCCTCTTGGCCGTGCGTCA |
| m-GAPDH | Forward | GAGAGACCCCACTTGCTGCCA |
| | Reverse | CTCACACTGCCCCTCCCTGGT |
| Z-AhR2 | Forward | GGGAAGGTGGTTCTTGGCTAC |
| | Reverse | CTCCTGTCTTTATCATTCTGATGTGGTT |
| zARNT2A | Forward | TTTGTCAGACCGCGGCGAAT |
| | Reverse | GTCCTCGTCGTCAAAATCCA |
| Z-Runx2a masns-isoform | Forward | CTCCCGCTTTAGGACTTCGA |
| | Reverse | GGAGTCACCGAGCTGAAAAGACT |
| Z-β-actin | Forward | CAACAGGGAAAAGATGACACAGAT |
| | Reverse | CAGCCTGGATGGCAACGT |
| Z-osteocalcin | Forward | TGGCCTCTATCATCATGAGACAGA |
| | Reverse | CTCTCGAGCTGAAATGGAGTCA |
| Z-osteopontin | Forward | CGCTCAGCAAGCAGTTCAGA |
| | Reverse | AGAATAGGAGGTGGCCGTTGA |
| Z-collagen 1α2 | Forward | GGAAACCTGAAGAAGGCTGTGT |
| | Reverse | TGAAAGTGAAGCGGCTGTTG |

time PCR (qRT-PCR), carried out with the SYBR qPCR kit (Kapa Biosystems). The specific primers used in the reactions are detailed in Table 1. Relative gene expression levels were calculated using the ΔΔCt method, normalized to β-actin as the reference gene, and presented as fold changes compared to control samples. All experiments were performed in triplicate to ensure reliability.

### 2.13 Statistical analysis

All data for each treatment are presented as mean ± SD based on at least three replicate results and the significant difference ($P < 0.05$) between groups was calculated by the paired $t$-test. All the analyses were performed using GraphPad Prism software.

## 3. Results and discussion

### 3.1 Morphological and size characterization of DEP

The prepared DEP solution was subjected to scanning electron microscopy (SEM) and energy-dispersive X-ray (EDX) analysis to determine its morphological and elemental properties. SEM imaging revealed that the average size of DEP in the culture medium stock solution was 31.95 ± 12.5 nm, classifying them within the particulate matter (PM) size range (Fig. 1A) (ESI Fig. 1, 2 and Tables 1, 2†). The surface morphology of DEP was observed to be non-uniform, with particles exhibiting a predominantly spherical shape. These spherical particles tended to aggregate, forming larger clusters. EDX analysis at two distinct spots on the DEP surface confirmed the presence of multiple elements, including carbon, nickel, copper, bromine, lead, chromium, and sulfur. These elements are known components of gaseous particulate matter that contribute significantly to air pollution and its associated health hazards (Fig. 1B). The particle size plays a crucial role in their biological impact. Smaller particles, such as the observed

DEP, can penetrate deep into the body without activating immune responses that typically work to eliminate foreign substances. This characteristic makes such particles particularly harmful as they can infiltrate sensitive tissues and organs, potentially leading to systemic health effects. The physico-chemical properties of DEP provide the foundation for our investigation into their impact on bone formation and remodeling in Zebrafish and *in vitro* osteoblast models. In line with the findings of,[22] which showed that the toxicity of diesel particles varies with their physicochemical characteristics, our study emphasizes the importance of these properties in influencing biological effects. Similar efforts have been made in the past to determine the chemical composition and size of the diesel engine emissions[23] which indicated the presence of fine particles like PM2.5.

### 3.2 Effect of DEP on pre-osteoblast cells (MC3T3-E1) *in vitro*

To evaluate the impact of diesel exhaust particles (DEP) on pre-osteoblast cells (MC3T3-E1), we assessed cell viability and osteoblast differentiation under *in vitro* conditions. Cells were exposed to varying concentrations of DEP (0, 50, 100, and 200 μg ml$^{-1}$), and their viability was measured using the MTT assay, alongside morphological observations similar to other relevant studies.[24,25] The results showed no significant toxicity across the tested DEP concentrations. Morphological analysis (Fig. 2A) demonstrated that the cells maintained a normal structure, with no noticeable changes in shape or adherence properties. Similarly, the MTT assay results (Fig. 2B) indicated no significant reduction in cell viability, suggesting that DEP does not exert cytotoxic effects at these concentrations. In contrast, other studies[26,27] reported that DEP particles can induce cytotoxicity by regenerating reactive oxygen species (ROS) formation and causing oxidative stress.
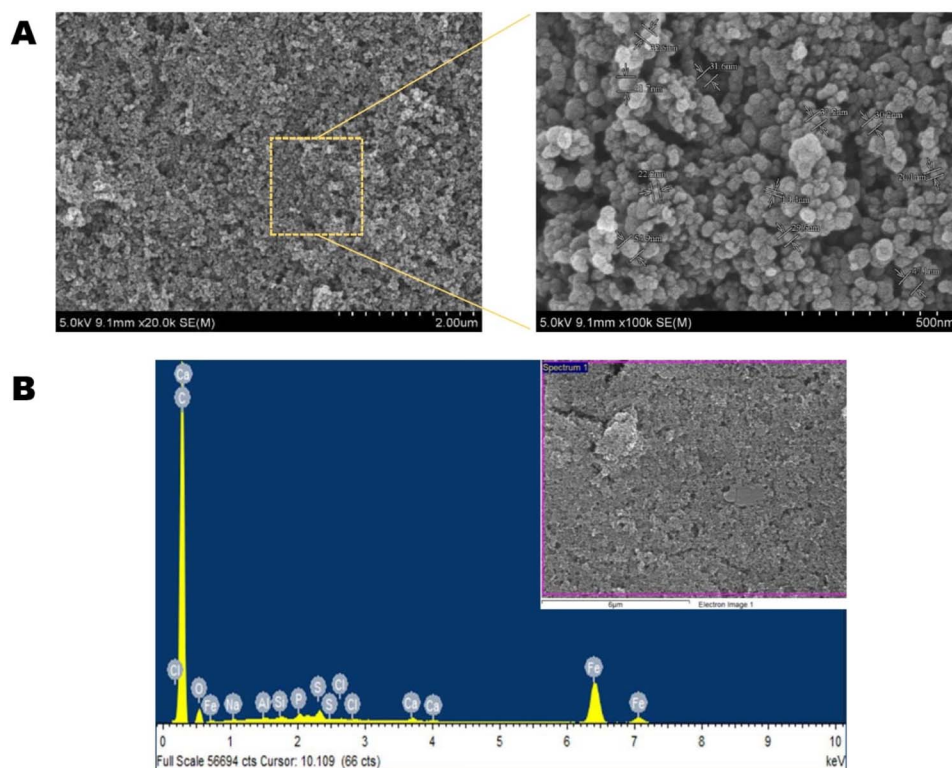
Fig. 1 (A) High-resolution SEM images showing the size and surface morphology of diesel exhaust particles collected from diesel engine exhaust. (B) EDX analysis results indicate the elemental composition of DEP, highlighting the presence of pollutants such as nickel, lead, and sulfur.
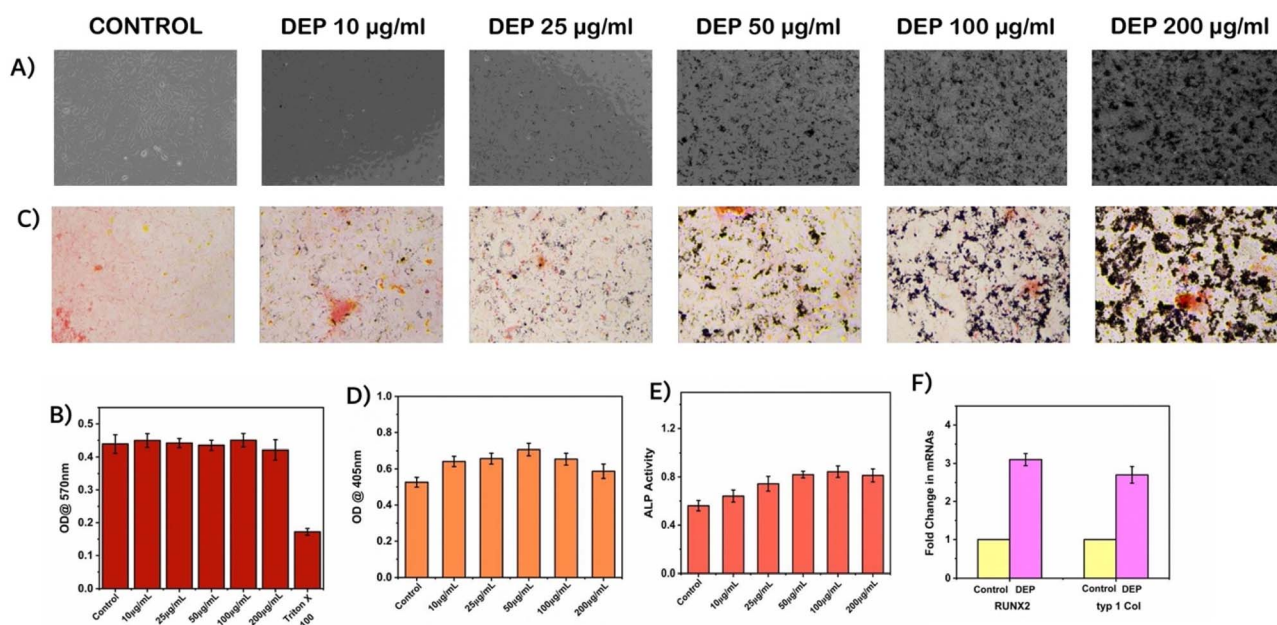


Fig. 2 Effect of diesel exhaust Particles (DEP) on MC3T3-E1 pre-osteoblast cells. (A) Microscopic images of MC3T3-E1 cells treated with varying concentrations of DEP (0, 50, 100, and 200 $\mu$g ml$^{-1}$) show no significant changes in cell viability count as indicated at OD at 570 nm. (B) MTT assay results indicate cell viability after exposure to different concentrations of DEP, demonstrating no cytotoxic effects. (C and D) Alizarin Red staining depicting calcium deposition in DEP-treated cells. DEP concentrations of 25–50 $\mu$g ml$^{-1}$ showed the highest calcium deposition compared to the control. (E) ALP activity analysis indicated increased enzymatic activity in DEP-treated cells, with higher activity observed across all DEP concentrations compared to the control. (F) Real-time RT-PCR analysis of osteoblast markers, Runx2 and type 1 collagen, showing significant upregulation at 50 $\mu$g ml$^{-1}$ DEP compared to the control, highlighting DEP's osteogenic potential.

### 3.3 Effect of DEP on calcium deposition, ALP activity, and osteoblast marker expression

To further explore the osteogenic potential of DEP, MC3T3-E1 cells were exposed to varying DEP concentrations for 7 days, and calcium deposition, alkaline phosphatase (ALP) activity, and osteoblast marker expression were assessed. Calcium deposition, a hallmark of osteoblastic activity, was evaluated using Alizarin Red staining (Fig. 2C and D). The results revealed a significant increase in calcium deposition at DEP concentrations ranging from 25 to 200 $\mu g\ ml^{-1}$ compared to the control. Concentrations of 25 to 50 $\mu g\ ml^{-1}$ exhibited the highest levels of calcium deposition compared to other concentrations. ALP activity, a key indicator of osteoblast maturation, was assessed (Fig. 2E). DEP exposure led to a consistent increase in ALP activity across all concentrations compared to the control, supporting the role of DEP in promoting osteoblastic differentiation. At the molecular level, real-time RT-PCR analysis was conducted to evaluate the expression of osteoblast-specific markers, Runx2 and type 1 collagen (Fig. 2F). Both markers showed significant upregulation at a DEP concentration of 50 $\mu g\ ml^{-1}$ compared to the control. This suggests that DEP enhances the transcriptional activity of key genes involved in osteoblast differentiation and extracellular matrix formation. The formation of bright nodules, indicative of mineralized matrix development, was observed in DEP-treated osteoblasts.

This indicates that DEP promotes osteoblastic activity and facilitates the deposition of hydroxyapatite crystals, a critical component of the extracellular matrix during bone formation. These findings demonstrate the potential role of DEP in osteoblast differentiation and mineral deposition. DEP enhances calcium deposition, ALP activity, and the expression of osteogenic markers. A higher activity of early-stage bone markers[28] indicates its capacity to promote new bone formation. These results collectively demonstrate the ability of DEP to promote osteoblastic activity and mineral deposition *in vitro*. However, many studies have reported a negative association between air pollution and bone mineral density and formation[29] highlighting the complexity of DEP's impact on bone health under varying conditions.

### 3.4 Toxicity evaluation of DEP in zebrafish embryos and larvae

To better understand the impact of DEP on human bone health, it is crucial to examine findings from model organisms like Zebrafish, which play a vital role in toxicology research.[30] To assess the toxicity of diesel exhaust particles (DEP), zebrafish embryos were exposed to varying concentrations (0, 50, 100, and 200 $\mu g\ ml^{-1}$) for up to 84 hours. Morphological images were captured using a stereomicroscope at 12 and 84 hours (Fig. 3A). The results showed no significant morphological changes
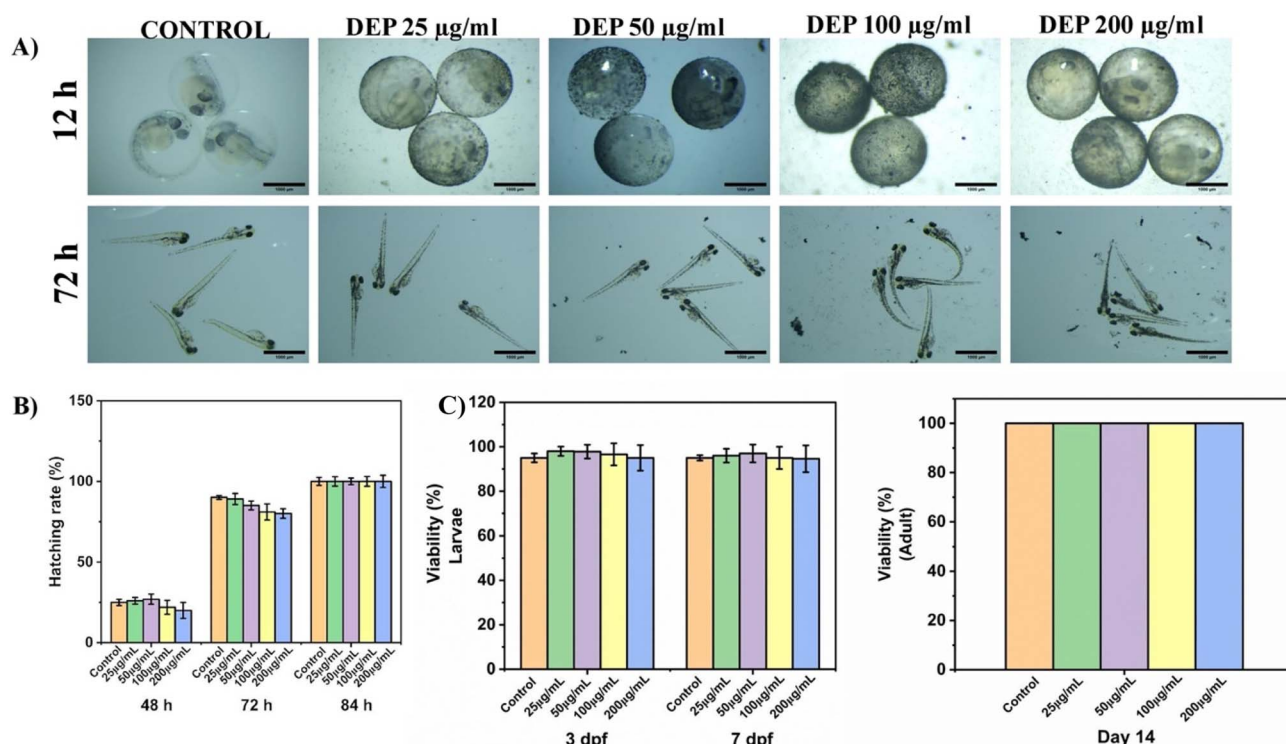


**Fig. 3** Toxicity assessment of diesel exhaust particles (DEP) in Zebrafish embryos and larvae. (A) Morphological images of zebrafish embryos and larvae treated with varying concentrations of DEP (0, 50, 100, and 200 $\mu g\ ml^{-1}$) for 12 and 72 hours, showing no significant abnormalities across groups. (B) Hatching rates of zebrafish embryos exposed to different concentrations of DEP at 48, 72, and 84 hours. No significant changes were observed, with a slight decrease at 72 hours in the 200 $\mu g\ ml^{-1}$ group. (C) Viability of zebrafish larvae treated with DEP until 7 days post-fertilization (dpf), demonstrating no significant reduction in survival across all tested concentrations. (C) Viability of adult zebrafish treated with DEP for 14 days, demonstrating no significant reduction in survival across all tested concentrations.

across the treatment groups, indicating the absence of visible developmental abnormalities.

The hatching rate of the embryos was calculated at multiple time points (48, 72, and 84 hours post-exposure; Fig. 3B). No significant differences were observed in the hatching rates across the DEP concentrations. However, a slight decrease in hatching was noted at 72 hours in the 100–200 μg ml⁻¹ group compared to the control, suggesting minimal impact at high concentrations. Toxicity was further assessed in zebrafish larvae treated with DEP for 7 days. The viability of the larvae was evaluated, and the results (Fig. 3C) revealed no significant reduction in viability across all tested DEP concentrations (0–200 μg ml⁻¹). These findings suggest that DEP exposure at these concentrations does not induce acute toxicity in zebrafish embryos or larvae. Additionally, 100% viability was observed in adult zebrafish with different concentrations of DEP exposure up to 14 days (Fig. 3D).

### 3.5 Evaluation of bone mineralization in zebrafish larvae treated with DEP

To investigate the osteogenic effects of DEP, Zebrafish larvae were treated with various DEP concentrations for 7 days, and bone mineralization was assessed using Alizarin Red S staining, a calcium-binding stain that highlights mineralized areas in bone tissue. The results provided a visual representation of calcium mineralization in the skull and vertebral regions after 15 minutes of staining (Fig. 4A and B). The data revealed a significant increase in bone mineralization in DEP-treated larvae, particularly in the skull and vertebral regions, up to a concentration of 25 μg ml⁻¹. This suggests that low concentrations of DEP promote mineral deposition in the extracellular matrix during osteogenesis. However, at higher concentrations (100 μg ml⁻¹), a decrease in bone mineralization was observed, especially in the vertebral region. These findings indicate that while low concentrations of DEP may enhance bone mineralization, higher concentrations could have inhibitory effects. This biphasic response underscores the importance of optimizing DEP concentrations for potential applications in bone regeneration studies. In a related study,[31] found that PM2.5 exposure did not affect cell viability through proliferation and apoptosis, but it significantly inhibited osteoblast differentiation in a dose-

dependent manner. Moreover, the results suggest that DEP does not induce significant toxicity in zebrafish embryos or larvae at tested concentrations. Low concentrations of DEP promote bone mineralization, highlighting their potential role in osteogenesis while higher concentrations may hinder mineral deposition. This calls for further investigation into the dose-dependent effects and underlying mechanisms of DEP on bone development and regeneration.

### 3.6 Effect of DEP on the zebrafish scale regeneration model

We investigate the effects of DEP on scale regeneration in healthy zebrafish. Regenerated scales were collected after 7 days of exposure to varying concentrations of DEP (0, 25, 50, and 100 μg ml⁻¹) and analyzed using different staining techniques to evaluate calcium deposition, mineral density, and distribution. Alizarin Red staining (Fig. 5A and B) and Calcein staining (Fig. 5C and D) were employed to evaluate calcium deposition and mineralization in the regenerated scales to quantify the new bone matrix deposited.[32] Both staining methods revealed significant increases in calcium deposition at DEP concentrations of 25 to 50 μg ml⁻¹ compared to the control group. However, at 100 μg ml⁻¹, calcium deposition was notably reduced, suggesting a concentration-dependent response to DEP exposure. Von Kossa staining (Fig. 5E and F) as described in (ref. 33), which highlights phosphate-rich mineral deposits, demonstrated increased mineral density in the 25 to 50 μg ml⁻¹ DEP-treated groups, while a reduction in mineralization was observed at 100 μg ml⁻¹. Similarly, Alcian Blue staining (Fig. 5G and H), used to identify acidic polysaccharides, showed consistent mineral density changes that corroborated the findings from Alizarin Red and Von Kossa staining. The expression of key osteoblast markers, Runx2 and type 1 collagen, was analyzed using real-time RT-PCR (Fig. 5I). Results indicated a significant upregulation of these markers at 25 to 50 μg ml⁻¹ DEP concentrations, highlighting enhanced osteoblastic activity and bone formation. Conversely, a decrease in marker expression was observed at 100 μg ml⁻¹ DEP exposure, suggesting inhibitory effects on osteoblast differentiation and activity at higher DEP concentrations.

These findings indicate that DEP exposure at lower concentrations (25–50 μg ml⁻¹) promotes calcium deposition and mineralization during zebrafish scale regeneration, potentially
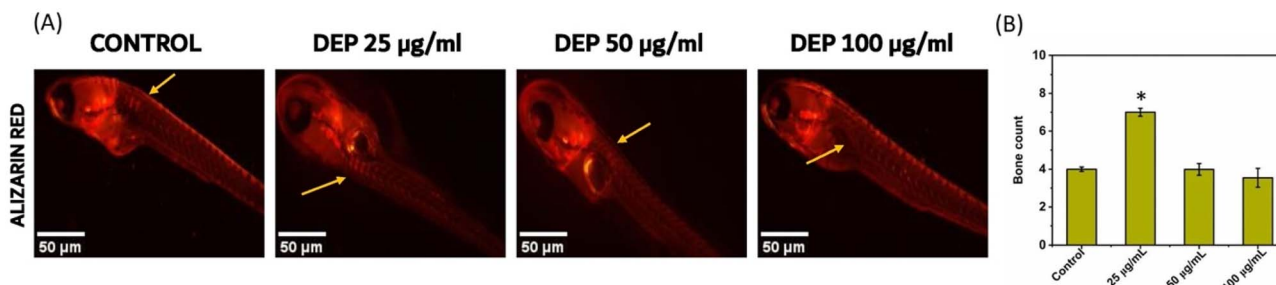


**Fig. 4** Effect of diesel exhaust particles (DEP) on Bone mineralization in zebrafish larvae. (A) Alizarin Red S staining of zebrafish larvae treated with varying concentrations of DEP (0, 25, 50, and 100 μg ml⁻¹) for 7 days. Images depict calcium mineralization in the skull and vertebral regions, with enhanced mineralization observed at 25 μg ml⁻¹. (B) Quantification of bone mineralization in zebrafish larvae, indicating a significant increase at 25 μg ml⁻¹ DEP compared to the control. A decrease in mineralization was noted at 100 μg ml⁻¹, particularly in the vertebral region. Expressed as mean ± SD. * indicates a statistically significant increase compared to controls ($P < 0.05$).
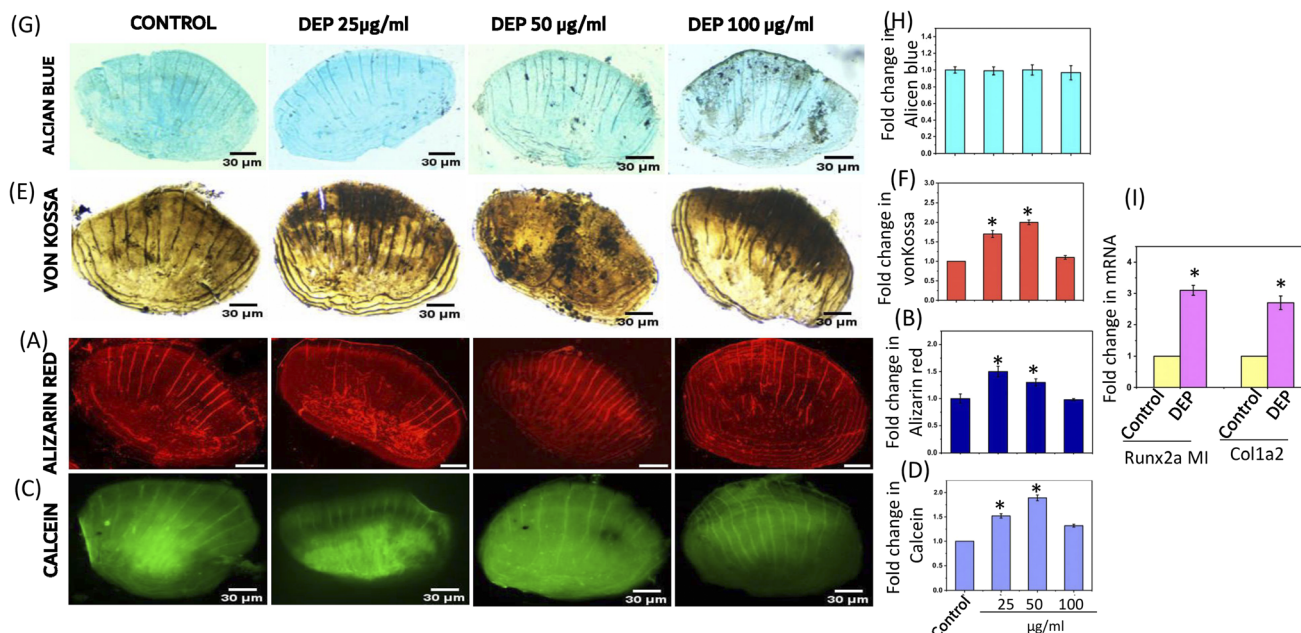
Fig. 5 Effect of DEP on scale regeneration in zebrafish. (A and B) Alizarin Red staining showing calcium deposition in regenerated scales of zebrafish treated with varying concentrations of DEP (0, 25, 50, and 100 μg ml$^{-1}$). Calcium deposition increased significantly at 25–50 μg ml$^{-1}$ DEP and decreased at 100 μg ml$^{-1}$ (C and D) Calcein staining highlights calcium mineralization in the regenerated scales, with the highest mineralization observed at 25–50 μg ml$^{-1}$ DEP concentrations (E and F) Von Kossa staining demonstrating phosphate-rich mineral deposits in scales, indicating enhanced mineral density at 25–50 μg ml$^{-1}$ and reduced mineralization at 100 μg ml$^{-1}$ (G and H) Alcian Blue staining representing acidic polysaccharides in the regenerated scales, showing similar trends of increased mineral density at 25–50 μg ml$^{-1}$ and decreased mineralization at 100 μg ml$^{-1}$ DEP. (I) Real-time RT-PCR analysis of osteoblast markers, Runx2 and type 1 collagen, showing significant upregulation at 25–50 μg ml$^{-1}$ DEP and a reduction at 100 μg ml$^{-1}$ DEP exposure. Expressed as mean ± SD. * indicates a statistically significant increase compared to controls ($P < 0.05$).

enhancing osteoblastic activity. The increased expression of Runx2 and type 1 collagen further supports the osteogenic potential of DEP at these concentrations. However, higher concentrations (100 μg ml$^{-1}$) exhibit adverse effects, leading to reduced mineral density and osteoblast marker expression, likely due to toxicity or disrupted cellular pathways. The dose-dependent effects observed in this study emphasize the importance of optimizing DEP exposure levels for potential therapeutic applications in bone regeneration. These findings align with other studies reporting that toxic pollutants from smoke or atmosphere exert dose and duration dependent effects by suppressing and inhibiting osteoblast and osteoclast activity through the activation of alternative signaling pathways.[34] While low concentrations may have osteogenic benefits, higher concentrations pose risks that warrant further investigation to elucidate the underlying mechanisms and long-term effects of DEP on bone tissue. This effect could also be attributed to the physiochemical properties of the DEPs which influence cell particle interactions and trigger biological response.[35]

### 3.7 Effect of DEP on scale regeneration in osteoporotic zebrafish

To assess the effects of DEP on scale regeneration in osteoporotic zebrafish, dexamethasone was used to induce osteoporotic conditions. Zebrafish were then exposed to varying concentrations of DEP (0, 25, 50, and 100 μg ml$^{-1}$) for 7 days. Regenerated

scales were analyzed using Alizarin Red staining for calcium deposition, along with molecular and enzymatic assays to evaluate osteoblast and osteoclast activity. Alizarin Red staining (Fig. 6A and B) showed a significant decrease in calcium deposition in DEP-treated groups at concentrations of 25 to 100 μg ml$^{-1}$ compared to the control. This reduction in calcium deposition suggests impaired mineralization in osteoporotic zebrafish treated with DEP, even at lower concentrations. Similarly, real-time RT-PCR analysis revealed a significant decrease in the expression of key osteoblast markers, including Runx2 (Fig. 6C), type 1 collagen (Fig. 6D), osteocalcin (Fig. 6E), and osteonectin (Fig. 6F), in DEP-treated groups (25–100 μg ml$^{-1}$). Alkaline phosphatase (ALP) activity, a marker of osteoblast maturation, was also significantly reduced in DEP-treated zebrafish at concentrations of 25 to 100 μg ml$^{-1}$ (Fig. 6G). This further supports the inhibitory effects of DEP on bone-forming activity.

The Ca/P ratio (Fig. 6H), indicative of bone mineral composition, was significantly decreased in DEP-treated groups compared to the control, further emphasizing the detrimental effects of DEP (25 to 100 μg ml$^{-1}$) on bone mineralization under osteoporotic conditions. In contrast, tartrate-resistant acid phosphatase (TRAP) activity, a marker of osteoclast activity, was significantly increased in DEP-treated groups (25–100 μg ml$^{-1}$) compared to the control (Fig. 6I). This suggests that DEP exposure promotes osteoclast activity, potentially contributing to increased bone resorption under osteoporotic conditions.
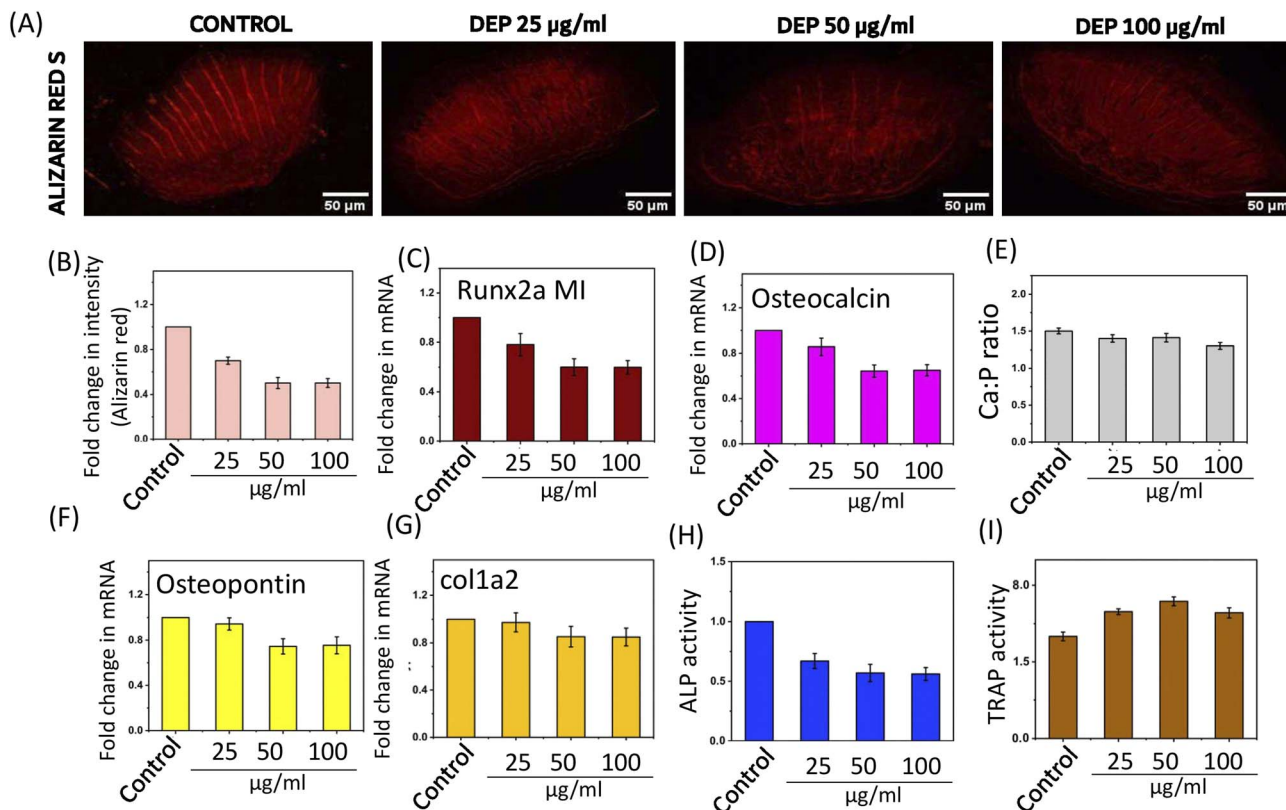
Fig. 6   Effect of DEP on scale regeneration in osteoporotic zebrafish. (A and B) Alizarin Red staining showing calcium deposition in regenerated scales of zebrafish treated with DEP (0, 25, 50, and 100 μg ml$^{-1}$). Calcium deposition was significantly decreased in all DEP-treated groups compared to the control. (C) Fold change in Runx2 mRNA expression analyzed by real-time RT-PCR, demonstrating a reduction in osteoblast differentiation at DEP concentrations of 25–100 μg ml$^{-1}$. (D) Fold change in type 1 collagen mRNA expression, showing decreased collagen production with DEP exposure. (E and F) Fold changes in osteocalcin and osteonectin mRNA expression, respectively, both of which were significantly reduced in DEP-treated groups. (G) ALP activity in regenerated scales, highlighting a decrease in osteoblast maturation across all DEP concentrations. (H) Ca/P ratio of regenerated scales, showing reduced bone mineral composition in DEP-treated groups compared to the control. (I) TRAP activity, a marker of osteoclast activity, showing a significant increase in DEP-treated groups, suggesting enhanced bone resorption.

The results demonstrate that DEP exposure at 25–50 μg ml$^{-1}$ promotes bone formation under healthy conditions but negatively affects bone formation in osteoporotic zebrafish. At higher concentrations (100 μg ml$^{-1}$), DEP consistently inhibits bone formation in both healthy and osteoporotic conditions. The decrease in osteoblast marker expression and ALP activity, along with the increase in TRAP activity, suggests that DEP exposure disrupts the balance between bone formation and resorption, particularly in osteoporotic conditions through cytokines.[36] These findings highlight the dual role of DEP, with potential osteogenic benefits at lower concentrations in healthy conditions but adverse effects under osteoporotic or high-dose conditions. Further studies are required to elucidate the underlying molecular mechanisms and evaluate the long-term impact of DEP on bone metabolism.

### 3.8   Effect of DEP on bone fracture healing in zebrafish fin fracture models: healthy and osteoporotic conditions

The study aims to investigate the bone fracture healing of the injury created in the fin region of adult zebrafish. To comprehensively assess how DEP affects the osteogenic property, we employed an *in vivo* zebrafish fin fracture model. This approach allowed us to scrutinize the osteoinductive properties of DEP by observing the fin's response to treatment at various concentrations, given that bone callus mineralization is a hallmark characterized by osteoblastic calcium deposition. The Zebrafish fin was fractured in both healthy and osteoporotic zebrafish and subjected to DEP treatment. The evaluation was conducted on day 7 after the initial injury. Our results unequivocally demonstrated that DEP holds osteoinductive property of DEP at 25–50 μg ml$^{-1}$ concentration, effectively triggering fin bone restoration during the 7 days observation in healthy adults (Fig. 7A and B). The steady progression in fin remodeling underscores the bone-forming capacity of DEP, significantly impacting skeletal callus formation at the injured fin region. The region was then stained with the alizarin red stain to check for callus formation and mineralization. This figure portrays the healing of zebrafish fins treated with DEP. The appearance of calcified nodules at the reconstructed fin site serves as a clear indicator that DEP has some osteoinductive properties that actively stimulate osteoblastic activity, leading to calcium deposition within the bone callus region. Whereas in osteoporosis induced DEP
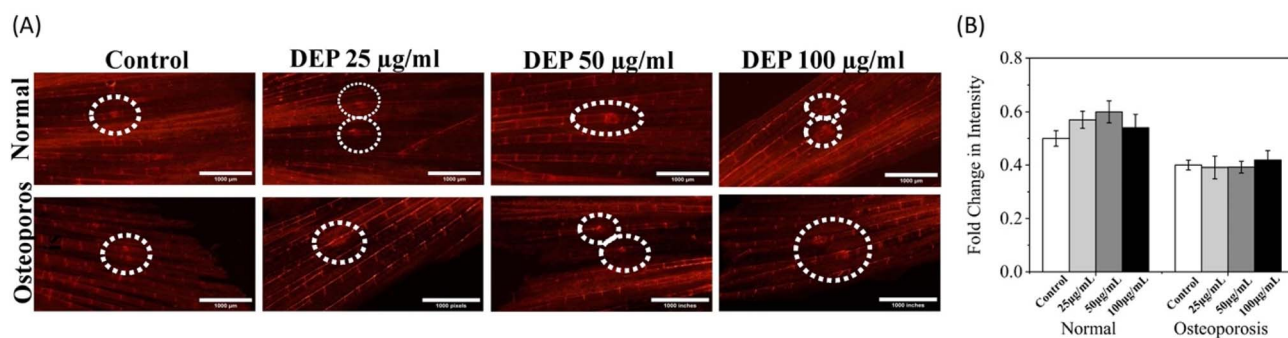
**Fig. 7** (A) Images of the injured tail region stained with alizarin red. The circled region indicates the callus formation. It shows the wound healing trajectory in both normal and osteoporosis-induced zebrafish. (B) This graph illustrates the mean intensity in the tail region of zebrafish, treated with control, 50, 100, and 200 μg ml$^{-1}$ DEP. ns signify statistical non-significance compared to the control group ($p < 0.05$) and asterisk (*) signifies the significant difference in callus formation compared to the control group ($p < 0.05$).

treated adult ZF showed no significant changes in callus formation in the injured region compared with the control groups. This indicates that the healing process is delayed in osteoporosis-induced fishes in comparison with healthy fishes.

### 3.9 Axial bone density in adult zebrafish

A whole-mount Alizarin Red staining assay was employed to visualize calcium deposition in the axial skeletal area to evaluate the effect of DEP on bone formation in the vertebral region of adult zebrafish. The vertebral region of healthy and dexamethasone-induced osteoporotic zebrafish was examined 7 days post-treatment with varying concentrations of DEP (0, 25, 50, and 100 μg ml$^{-1}$). In healthy adult zebrafish, the staining intensity (Fig. 8A) revealed enhanced mineralization in the vertebral region at DEP concentrations of 25–50 μg ml$^{-1}$ compared to the control group. The bright red regions indicate substantial mineral deposits, suggesting an increase in osteoblastic calcium deposition. However, at a concentration of 100 μg ml$^{-1}$, no significant changes in mineralization were observed, indicating that higher concentrations of DEP may not further enhance bone formation or might begin to exhibit inhibitory effects. In dexamethasone-induced osteoporotic

zebrafish, DEP treatment did not result in significant increases in mineralization compared to the control group. The staining patterns in the vertebral region remained largely unchanged across all DEP concentrations (0–100 μg ml$^{-1}$), suggesting that the osteoporotic condition mitigates the osteoinductive effects of DEP. The findings highlight a dose-dependent effect of DEP on calcium deposition in the vertebral region of healthy adult zebrafish, with optimal bone mineralization observed at concentrations of 25–50 μg ml$^{-1}$. However, at higher concentrations (100 μg ml$^{-1}$), the osteogenic potential of DEP diminishes. Similarly, a study conducted on growing rats to evaluate whether diesel engine exhaust influences bone metabolism demonstrated a significant increase in bone mineral density and bone mineral content in the lumbar vertebra of exposed rats compared to the control group.[37] In contrast, DEP treatment in osteoporotic zebrafish failed to elicit significant changes in mineralization patterns. This indicates that the impaired bone microenvironment in osteoporosis may hinder the ability of DEP to promote bone formation. The results align with previous findings that suggest DEP exhibits osteoinductive properties under healthy conditions but is less effective in pathological states such as osteoporosis. This study
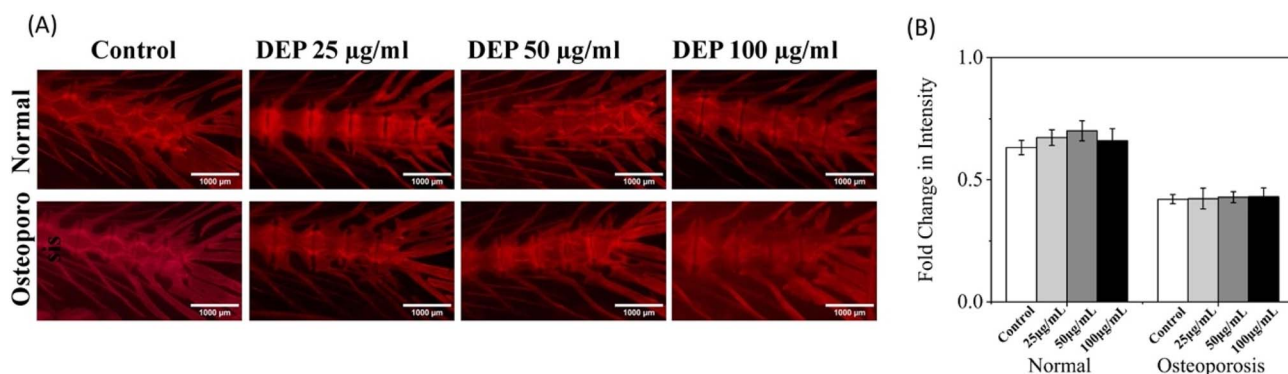


**Fig. 8** (A) The photograph shows the vertebral region of the normal adult zebrafish treated and osteoporosis-induced adult fish in various concentrations of DEP and stained with Alizarin red. The bright red region indicated the calcium deposition. (B) This graph illustrates the mean intensity in the vertebral region of zebrafish, treated with control, 50, 100, and 200 μg ml$^{-1}$ DEP. ns signify statistical non-significance compared to the control group ($p < 0.05$) and asterisk (*) signifies.

demonstrates that DEP can enhance bone mineralization in the vertebral region of healthy zebrafish at specific concentrations but is ineffective in promoting mineralization under osteoporotic conditions. These findings emphasize the need to consider the biological context when evaluating DEP as a potential osteogenic agent. Further research is necessary to elucidate the mechanisms underlying these effects and to optimize DEP-based applications for bone regeneration. Effective risk assessment of DEP in bone health requires biomarkers that are directly or indirectly associated with bone metabolism. However, this presents a challenge for complex mixtures like diesel exhaust, as the specific components driving changes in bone metabolism or structure remain largely unknown.[38]

### 3.10 DEP exacerbates bone remodeling in osteoporosis

In our study, DEP demonstrated good tolerance up to 200 μg ml$^{-1}$ in both *in vitro* (pre-osteoblastic cells) and *in vivo* models (Zebrafish embryos). Interestingly, DEP showed osteogenic properties by enhancing bone mineralization at a concentration of 25 μg ml$^{-1}$. However, at higher concentrations of 50 and 100 μg ml$^{-1}$, it inhibited mineralization in zebrafish larvae. A comparable trend was observed in the scale regeneration of treated zebrafish models. DEPs have been recognized for their estrogenic, anti-estrogenic, and anti-androgenic activities. The polycyclic aromatic hydrocarbons (PAHs) in diesel exhaust are established endocrine disruptors, known to target estrogen receptors and aryl hydrocarbon receptors (AhR). Endocrine-disrupting chemicals (EDCs), including DEPs, have been documented to exhibit osteogenic activity at lower doses. For example, Kanno *et al.* (2004) compared the effects of BPA, p-*n*-nonylphenol (NP), and bis(2-ethylhexyl)phthalate (DEHP) on M3T3-E1 preosteoblasts. While all three compounds reduced preosteoblast proliferation, only BPA (1 μM to 10 μM) enhanced alkaline phosphatase activity and increased cellular calcium content, suggesting it promoted early osteoblast differentiation.[39] DEP, similar to BPA, is known to interact with AhR, mediating its effects through both canonical and non-canonical pathways. To investigate this, we analyzed the expression profile of AhR2 in zebrafish skeletons following exposure to DEP (100 μg ml$^{-1}$). The results revealed a significant increase in AhR mRNA levels, confirming the receptor's involvement in DEP-mediated effects (Fig. 9A). AhR is a ligand-activated transcription factor that plays a pivotal role in bone remodeling by modulating the interaction between osteoblasts (bone-forming cells) and osteoclasts (bone-resorbing cells). Upon ligand binding, AhR-2 undergoes a conformational change that enables its translocation to the nucleus.[40] There, it forms a heterodimer with ARNT (Aryl Hydrocarbon Receptor Nuclear Translocator). The AhR-ARNT complex activates xenobiotic response elements (XRE), initiating the transcription of genes involved in immune response, toxicity, and bone remodeling.[41] Following this understanding, we further examined ARNT levels in DEP-exposed zebrafish models. Consistent with the AhR increase, zARNT2A expression also showed a significant upregulation upon DEP exposure (Fig. 9B). Air pollution has been implicated in poor bone health, including decreased bone
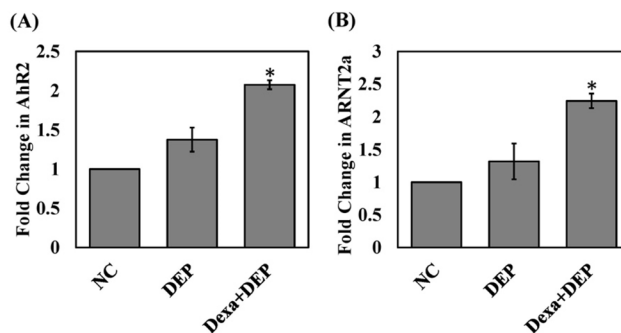


Fig. 9 Effect of DEP on AhR2 and ARNT2a mRNA expression levels. (A) AhR2 mRNA expression and (B) ARNT2a mRNA expression in zebrafish skeleton tissue. Results are presented as mean ± SEM. * indicates a statistically significant increase compared to controls ($P < 0.05$).

mineral density, delayed fracture healing, and disruption of hormonal pathways critical for osteogenesis. For instance, postmenopausal women with reduced estrogen levels often exhibit increased RANKL expression, contributing to bone loss.[42] Additionally, studies have demonstrated a negative correlation between air pollution indicators such as PM2.5 and PM10 and bone mineral density.[43] Similarly, our findings highlighted that higher DEP concentrations delayed scale regeneration, impaired fracture healing, and reduced axial bone quality. In osteoporotic conditions, DEP exacerbated these detrimental effects on bone regeneration and healing.

## 4. Conclusion

This study demonstrates that diesel exhaust particles (DEP) exert detrimental effects on bone health, depending on the concentration and physiological context. At low concentrations (25–50 μg ml$^{-1}$), DEP exhibits osteogenic potential by promoting calcium deposition, alkaline phosphatase activity, and upregulation of osteoblast markers, as observed in both *in vitro* and *in vivo* zebrafish models. However, higher concentrations of DEP (100 μg ml$^{-1}$ and above) negatively affect bone formation and mineralization, especially in osteoporotic zebrafish, by reducing osteoblast activity and promoting osteoclast-mediated bone resorption. DEP exposure also disrupted the bone regeneration process in pathological states, emphasizing its detrimental impact under compromised bone health conditions. Mechanistically, the involvement of aryl hydrocarbon receptor (AhR) pathways was evident in mediating DEP-induced effects on bone remodelling. These findings underscore the complex interaction between DEP, endocrine disruption, and bone metabolism. Overall, this study highlights the need for further exploration into DEP's dose-dependent effects, underlying molecular mechanisms, and long-term impact on bone health, particularly in vulnerable populations. Such insights will be instrumental in developing strategies to mitigate the adverse effects of air pollution on skeletal health. In conclusion, DEP-bound AhR interacts with ARNT to mediate detrimental effects on bone regeneration. At higher doses, elevated ARNT expression intensifies these detrimental

processes, thereby highlighting DEP's role in impaired bone health and regeneration. A key limitation is the lack of detailed morphometric data; since $PM_{2.5}$ can induce dose-dependent embryotoxicity with subtle shape changes and reduced hatching,[44] future work should quantify body length, cardiac function, and ROS.[45–47]

## Data availability

The data supporting this article have been included as part of the ESI† and Data are also available upon request from the authors.

## Author contributions

V. N.: writing – original draft preparation and methodology. S. Se., R. S.: methodology. V. S., S. Su.: conceptualization, writing – original draft preparation, supervision and validation.

## Conflicts of interest

The authors declare that they have no known competing financial interests or personal relationships that could have appeared to influence the work reported in this paper.

## Acknowledgements

## References

1 M. J. Wernke, in *Encyclopedia of Toxicology*, Elsevier, Oxford, 2014, pp. 111–114.

2 A. C. Lloyd and T. A. Cackette, *J. Air Waste Manag. Assoc.*, 2001, **51**, 809–847.

3 A. Sydbom, A. Blomberg, S. Parnia, N. Stenfors, T. Sandström and S. E. Dahlen, *Eur. Respir. J.*, 2001, **17**, 733–746.

4 E. Long and C. Carlsten, *Part. Fibre Toxicol.*, 2022, **19**, 11.

5 L. M. Barnhill, S. Khuansuwan, D. Juarez, H. Murata, J. A. Araujo and J. M. Bronstein, *Toxicol. Sci.*, 2020, **176**, 193–202.

6 Y. Tan, Z. Jia, Z. Deng and L. Li, *Interface Focus*, 2024, 7(14), 20230074.

7 T. Y. Choi, T. I. Choi, Y. R. Lee, S. K. Choe and C. H. Kim, *Exp. Mol. Med.*, 2021, **53**, 310–317.

8 S. Pasqualetti, G. Banfi and M. Mariotti, *J. Mol. Histol.*, 2012, **43**, 589–595.

9 M. Cecilia, *IOSR J. Environ. Sci. Toxicol. Food Technol.*, 2013, **5**, 67–70.

10 J. R. Fox, D. P. Cox, B. E. Drury, T. R. Gould, T. J. Kavanagh, M. H. Paulsen, *et al.*, *Air Qual. Atmos. Health*, 2015, **8**, 507–519.

11 F. K. Cayami, L. Claeys, R. de Ruiter, B. J. Smilde, L. Wisse, N. Bogunovic, *et al.*, *Sci. Rep.*, 2022, **12**, 14686.

12 A. Bernar, J. V. Gebetsberger, M. Bauer, W. Streif and M. Schirmer, *Int. J. Mol. Sci.*, 2022, **24**, 723.

13 S. Vimalraj, D. Govindarajan, S. Sudhakar, R. Suresh, P. Palanivel and S. Sekaran, *Int. J. Biol. Macromol.*, 2024, **259**, 1291–1303.

14 Y.-J. Dai, Y.-F. Jia, N. Chen, W.-P. Bian, Q.-K. Li, Y.-B. Ma, Y.-L. Chen and D.-S. Pei, *Environ. Toxicol. Chem.*, 2014, **33**, 11–17.

15 S. Vimalraj, S. Saravanan and R. Subramanian, *Chem.–Biol. Interact.*, 2021, **349**, 109667.

16 S. Zhai, C. Liu, S. Vimalraj, R. Subramanian, S. S. Abullais, S. Arora and S. Saravanan, *Peptides*, 2023, **163**, 171021.

17 M. J. Tomecka, L. P. Ethiraj, L. M. Sánchez, H. H. Roehl and T. J. Carney, *Dis. Model. Mech.*, 2019, **12**, dmm040258.

18 H. Sakata-Haga, M. Uchishiba, H. Shimada, T. Tsukada, M. Mitani, T. Arikawa, H. Shoji and T. Hatta, *Sci. Rep.*, 2018, **8**, 7453.

19 E. De Vrieze, L. Heijnen, J. R. Metz and G. Flik, *J. Appl. Ichthyol.*, 2012, **28**, 388–392.

20 S. Chaichit, T. Sato, H. Yu, Y. K. Tanaka, Y. Ogra, T. Mizoguchi and M. Itoh, *Pharmaceuticals*, 2021, **14**, 536.

21 D. C. Rio, M. Ares Jr, G. J. Hannon and T. W. Nilsen, *Cold Spring Harb. Protoc.*, 2010, **2010**, prot5439.

22 K. M. Bendtsen, L. Gren, V. B. Malmborg, *et al.*, *Part. Fibre Toxicol.*, 2020, **17**, 38.

23 P. K. Kanaujia, D. Singh, D. Tripathi, L. N. S. K. Konathala, S. Saran, R. K. Chauhan, *et al.*, *Anal. Lett.*, 2015, **48**, 2303–2318.

24 Q. Ge, S. Yang, Y. Qian, J. Chen, W. Yuan, S. Li, *et al.*, *Environ. Health Perspect.*, 2023, **131**, 107002.

25 M. Zhang, Y. Wang, R. M. S. Wong, K. K. L. Yung and R. Li, *Neurotoxicology*, 2022, **88**, 187–195.

26 Y. Sakurai, E. Oba, A. Honda, *et al.*, *Sci. Rep.*, 2024, **14**, 10503.

27 S. Steiner, C. Bisig, A. Petri-Fink and B. Rothen-Rutishauser, *Arch. Toxicol.*, 2016, **90**, 1541–1553.

28 S. Vimalraj, *Gene*, 2020, **754**, 144855.

29 D. Prada, G. López, H. Solleiro-Villavicencio, C. Garcia-Cuellar and A. A. Baccarelli, *Environ. Res.*, 2020, **185**, 109465.

30 K. Bambino and J. Chu, *Curr. Top. Dev. Biol.*, 2017, **124**, 331–367.

31 J. Yang, C. Han, J. Ye, X. Hu, R. Wang, J. Shen, L. Li, G. Hu, X. Shi, Z. Jia, X. Qu, H. Liu, X. Zhang and Y. Wu, *Toxicol. Lett.*, 2024, 127–139.

32 S. Pasqualetti, T. Congiu, G. Banfi and M. Mariotti, *Int. J. Exp. Pathol.*, 2015, **96**, 11–20.

33 M. R. Schneider, *Histochem. Cell Biol.*, 2021, **156**, 523–526.

34 R. Park, S. Madhavaram and J. D. Ji, *Cells*, 2020, **9**, 2294.

35 E. J. Park, J. Roh, M. S. Kang, S. N. Kim, Y. Kim and S. Choi, *PLoS One*, 2011, **6**, e26749.

36 X. Chen, Z. Wang, N. Duan, G. Zhu, E. M. Schwarz and C. Xie, *Connect. Tissue Res.*, 2018, **59**, 99–107.

37 N. Watanabe and T. Nakamura, *Arch. Environ. Contam. Toxicol.*, 1996, **30**, 407–411.

38 A. Morgott, *Crit. Rev. Environ. Sci. Technol.*, 2014, **44**(16), 1795–1864.

39 S. Kanno, S. Hirano and F. Kayama, *Toxicology*, 2004, **196**, 137–145.

40 Y. Miki, S. Hata, K. Ono, T. Suzuki, K. Ito, H. Kumamoto and H. Sasano, *Int. J. Mol. Sci.*, 2017, **18**, 2159.

41 D. W. Alhamad, H. Bensreti, J. Dorn, W. D. Hill, M. W. Hamrick and M. E. McGee-Lawrence, *J. Mol. Endocrinol.*, 2022, **69**, R109–R124.

42 D. Prada, G. Lopez, H. Solleiro-Villavicencio, C. Garcia-Cuellar and A. A. Baccarelli, *Environ. Res.*, 2020, **185**, 109465.

43 K. Alver, H. E. Meyer, J. A. Falch and A. J. Sogaard, *Osteoporos. Int.*, 2010, **21**(10), 1751–1760.

44 J. Duan, H. Hu, Y. Zhang, L. Feng, Y. Shi, M. R. Miller and Z. Sun, *Chemosphere*, 2017, **180**, 24–32.

45 K. M. Bendtsen, L. Gren, V. B. Malmborg, *et al.*, *Part. Fibre Toxicol.*, 2020, **17**, 38.

46 K. M. Bendtsen, A. Brostrom, A. J. Koivisto, I. Koponen, *et al.*, *Part. Fibre Toxicol.*, 2019, **16**(1), 23.

47 K. M. Bendtsen, C. H. F. Hansen, L. Krych, K. Skovgaard, *et al.*, *PLoS One*, 2017, **12**(5), e0176662.